Microchimica Acta (2019) 186: 430
https://doi.org/10.1007/s00604-019-3566-7

ORIGINAL PAPER

Photoelectrochemical aptasensing of ofloxacin based on the use of a TiO_2 nanotube array co-sensitized with a nanocomposite prepared from polydopamine and Ag_2S nanoparticles

Xiaofei Qin[1] · Liping Geng[1] · Qianqian Wang[1] · Yan Wang[1]

Received: 19 March 2019 / Accepted: 28 May 2019 / Published online: 11 June 2019

Abstract

A photoelectrochemical (PEC) method is described for aptamer-based detection of ofloxacin (OFL). It is making use of a TiO_2 nanotube array (NTA) that is sensitized with a structure composed of polydopamine and silver sulfide nanoparticles. The NTA were prepared by a two-step synthetic method. First, the TiO_2 nanotube electrode was covered with Ag_2S nanoparticles via successive ionic layer adsorption and reaction strategy. Next, they were coated with a thin film of polydopamine (PDA) by in-situ polymerization. The inorganic/organic nanocomposites exhibit distinctly enhanced visible-light PEC activity. This was exploited to fabricate a PEC aptasensor. The PDA film serves as both the sensitizer for charge separation and as a support to bind the aptamer against OFL. The aptasensor undergoes a decrease in photocurrent due to the formation of the aptamer-OFL complex. Under the optimized conditions and at a typical working potential of 0 V (vs. Hg/Hg_2Cl_2), the NTA has a linear response in the 5.0 pM to 100 nM OFL concentration range and a 0.75 pM detection limit (at $S/N = 3$). The aptasensor was successfully applied to the determination of OFL in spiked milk samples.

Keywords Inorganic/organic nanocomposite · Sensitization · Aptasensor · Antibiotic detection · Food sample

Introduction

Photoelectrochemical aptasensing has attracted considerable interest owing to its good selectivity, low cost and high sensitivity [1]. Photoelectrochemical (PEC) detection possesses the advantages of both electrochemical and optical analysis [2]. Compared to other biological recognition elements such as antibodies, aptamers show distinct advantages, including high target specificity, good chemical stability, easy production and low cost [3].Therefore, aptamers have been used as recognition receptor to fabricate aptamer-based sensors [4]. PEC aptasensor, the highly sensitive PEC assay technique coupled aptamer as capturing agent, have brought out a new detection platform for specific determination of various target analytes [5–8].

In PEC aptasensor construction, the photoactive material plays an important role in transducing the signal generated from photo-to-current and immobilizing aptamer molecules. As one-dimensional (1D) semiconductor nanomaterial, TiO_2 nanotube arrays (TiO_2 NTs) possess excellent PEC performances due to their large internal surface area for enhanced light absorption and well-defined 1D channel for promoted electrical carrier transport. However, the intrinsic wide band gap of TiO_2 (3.2 eV) results in the poor visible light absorption and low photo-to-current ability under visible light illumination, which restricts its applications [9]. Therefore, various methods have been made to improve the visible-light PEC activity of the TiO_2 NTs by promoting visible light absorption and photo-excited charge separation. Up to date, a series of work has been carried out on narrow-gap inorganic

Electronic supplementary material The online version of this article (https://doi.org/10.1007/s00604-019-3566-7) contains supplementary material, which is available to authorized users.

✉ Yan Wang
fagong@sdu.edu.cn

[1] College of Chemistry, Chemical Engineering and Materials Science, Collaborative Innovation Center of Functionalized Probes for Chemical Imaging in Universities of Shandong, Key Laboratory of Molecular and Nano Probes, Ministry of Education, Shandong Provincial Key Laboratory of Clean Production of Fine Chemicals, Shandong Normal University, Jinan 250014, People's Republic of China

semiconductor co-sensitized TiO_2 to enhance absorption in the visible range, such as CdTe/CdS/TiO_2 [10], PbS/CdS/TiO_2 [11], and so on. It is well proved that co-sensitization can improve the photoelectric conversion efficiency comparing to single sensitization. However, the proposed co-sensitization composites possess potential toxicity and instability which limits its application for PEC biosensor. Therefore, it is highly desired to develop new co-sensitized TiO_2 composites with merits such as high-efficiency photoelectric conversion, low toxicity and stability. As an important chalcogenide semiconductor, Ag_2S nanoparticle has attracted much interest owing to its narrow band-gap (1.0 eV) and high absorption coefficients. Besides, it possesses negligible toxicity compared to other commonly used narrow band gap materials such as CdS and PbS, making it a promising photoactive material [12]. Moreover, the conduction band (CB) of Ag_2S is less anodic than that of TiO_2, so that the photogenerated electrons in Ag_2S can be easily injected into the CB of TiO_2 due to the match in the energy level of Ag_2S with that of TiO_2.Therefore, Ag_2S nanoparticles sensitized TiO_2NTs composites (Ag_2S/TiO_2 NTs) can not only expand the absorption range of visible light but also improve the separation of photogenerated electron–hole pairs, which have been used as photocatalysis for water splitting [13] and phenol photodegradation [14]. Polydopamine (PDA) is a polymer derived from the self-polymerization of dopamine in slightly alkaline aqueous solution. It can be easily coated on various organic and inorganic substrates [15]. PDA film has also been explored as a unique dye in dye-sensitized solar cell because it possesses broadband light absorption and many conjugated polymer chains. These favor the photogenerated charge separation. Hence, PDA acts as excellent organic sensitizer for constructing photoactive composite material [16]. Moreover, PDA can be used for direct immobilization of biomolecule such as protein and nucleic acid via Michael addition or Schiff base reaction due to the presence of abundant reactive groups [17]. Compared to the conventional PEC constructing methods, the methodology of biosensor construction utilizing PDA exhibits the advantages of easier preparation, uniform coating, and biocompatible matrix to immobilize more biorecognition elements [18]. Thus, we firstly reported the preparation and application of PDA/Ag_2S co-sensitized TiO_2NTs ternary inorganic/organic photoactive nanocomposites for fabrication of novel PEC aptasensor.

It is well known that antibiotics have been extensively used as veterinary drugs to cure bacterial infections and improve growth rate of livestock. However, overuse of antibiotics may cause the accumulation of antibiotics in animal products which can enter the food chain and potentially result in a risk to human health such as toxic effect, allergic reaction and bacterial resistance [19, 20]. In order to ensure human food safety, many countries have set the maximum residue limits (MRL) of antibiotics in food products. For example, Japan has adopted a MRL value of 10 ppb for ofloxacin (OFL) in animal products [21]. Hence, the development of sensitive analytical methods to detect trace levels of OFL residue in animal food is highly desirable. Up to now, various analytical approaches have been developed to detect OFL, such as capillary electrophoresis [22], desorption corona beam ionization-mass spectrometry (DCBI-MS) [23], Ultra-high performance liquid chromatography-tandem mass spectrometry (UHPLC–MS/MS) [24], chemiluminescence method [25], electrochemical technique [26–28], colorimetric analysis [29], and fluorescent detection [30]. However, each of these methods suffers from at least one undesirable limitation, such as limited selectivity, low sensitivity, expensive instruments, operational complexity, high cost and long detecting time.

PEC aptasensors appear to be suitable complementary analytical tools for the determination of OFL at low concentrations owing to their excellent features. However, to the best of our knowledge, the preparation and application of PEC aptasensor for the detection of OFL have never been reported in the literature. Thus, we reported the first ofloxacin PEC aptasensor on the basis of PDA/Ag_2S/TiO_2 NTs nanocomposites. The ternary photoactive nanohybrids were prepared by a two-step synthetic method. First, the TiO_2 nanotube electrode was covered with Ag_2S nanoparticles via successive ionic layer adsorption and reaction strategy. Next, they were coated with a thin film of PDA by in situ polymerization. The obtained inorganic/organic nanocomposites exhibited distinctly enhanced visible-light PEC activity. The introduced PDA thin film acts simultaneously as a unique organic sensitizer to further enhance photo-to-current conversion efficiency of inorganic Ag_2S/TiO_2NTs semiconductor as well as a functional layer for direct attachment of more aptamers due to its uniform coating, large surface area, and abundant reactive groups. As illustrated in Scheme 1, aptamers were successfully attached to the PDA/Ag_2S/TiO_2 NTs electrode by Michael addition reaction between PDA and thiol groups of the aptamer [17]. After OFL was captured by the aptamer due to the specific recognition reaction, the photocurrent decreased with the increasing of aptamer-OFL bioaffinity complexes. The variation of photocurrent was used as monitoring signal for the detection of OFL. This novel visible-light driven PEC aptasensor was successfully applied to ultra-sensitively detect OFL with a detection limit of 0.75 pM, which was much lower than the previous reports for OFL detection using different analytical methods.

Experimental

Chemicals

Ofloxacin and 6-mercapto-1-hexanol (MCH) were obtained from Aladdin Reagent Co., Ltd. (Shanghai, China) (http://www.aladdin-e.com). Hydrofluoric acid, dopamine,

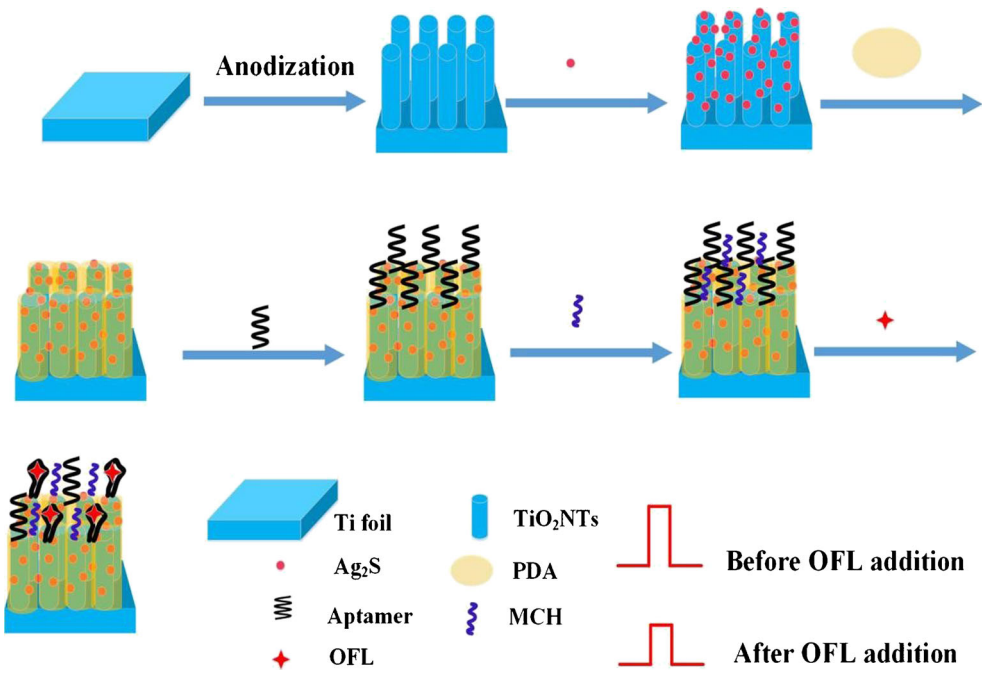

Scheme 1 Schematic illustration of the fabrication of the PEC aptasensor

silver nitrate, sodium sulfide, ascorbic acid were purchased from Sinopharm Chemical Reagent Co., Ltd. (Shanghai, China) (http://www.sinoreagent.com). The thiolated OFL binding aptamer was received from Sangon Biotech Co. Ltd. (Shanghai, China) (http://www.sangon.com) with the following sequences: 5'-SH-ATA CCA GCT TAT TCA ATT AGT TGT GTA TTG AGG TTT GAT CTA GGC ATA GTC AAC AGA GCA CGA TCG ATC TGG CTT GTT CTA CAA TCG TAA TCA GTT AG-3′.

Instruments

Scanning electron microscopy images were obtained on an S-4800 scanning electron microscope (Hitachi, Japan) (http://www.hitachi.com.cn). Fourier transform infrared spectra were recorded as KBr discs on an Alpha FT-IR spectrometer (Bruker, Germany) (https://www.bruker.com). X-ray diffraction patterns were measured by X-ray diffractometer (D8 advance, Bruker AXS, Germany) (https://www.bruker.com). The UV − visible spectrophotometer was used to measure UV–visible diffuse reflectance spectra (UV-2600, Shimadzu, Japan) (http://www.shimadzu.co.jp). Electrochemical impedance spectroscopy (EIS) was carried out with a CHI660D electrochemical workstation (Chenhua Instrument Shanghai Co., Ltd., China) (http://www.chinstr.com). A homemade PEC system was used for PEC measurements, including a 350 W xenon lamp with a 400 nm UV-cut filter as the visible light source and LK3200A electrochemical workstation (LANLIKE, Tianjin, China) (http://www.lanlike.com) used for recording photocurrent.

Preparation of PDA/Ag_2S/TiO_2NT electrode

Highly ordered TiO_2NTs were grown from Ti sheets (>99.8% purity) via electrochemical anodization of Ti slice (0.5 × 5.0 cm^2) with Pt counter electrode [31]. The anodic oxidation process was performed in an electrolyte of 0.5 wt% hydrofluoric acid at 20 V for 20 min. After being annealed at 450 °C with a 30 min hold, TiO_2 nanotubes were obtained.

The Ag_2S nanoparticles were deposited on the prepared TiO_2 NTs by the successive ionic layer adsorption and reaction (SILAR) method [32]. Firstly, the TiO_2 NTs electrode was dipped in the 0.05 M $AgNO_3$ aqueous solution for 1 min, then rinsed with distilled water and dried. Subsequently, the electrode was immersed in 0.05 M Na_2S aqueous solution for another 1 min, and washed with distilled water as well as dried. This procedure was repeated 4 cycles. The obtained electrode was noted as Ag_2S/TiO_2 NTs.

The PDA coated Ag_2S/TiO_2 NTs electrode was constructed by self-polymerization of DA in alkalescent aqueous solution under the optimized condition [15]. Typically, Ag_2S/TiO_2 NTs electrode was immersed in 0.01 M Tris-HCl buffer solution (pH 8.5) containing 3 mg·mL^{-1} dopamine and kept at room temperature for 2 h. Finally, the obtained PDA/Ag_2S/TiO_2 NTs electrode was washed by Tris-HCl buffer solution and stored in the 4 °C refrigerator for the following fabrication of aptasensor.

Construction of the PEC aptasensor

At first, the aptamer solution (20 μL, 2.0 μM) was placed onto the surface of the PDA/Ag_2S/TiO_2 NTs electrode at 4 °C for 12 h to form aptamer/PDA/Ag_2S/TiO_2NTs electrode. Then the

electrode was incubated with MCH solution (20 μL, 1 mM) for 60 min to obstruct the nonspecific binding region of electrode. After every immobilizing step, the electrode was washed thoroughly with Tris-HCl buffer. The constructed aptasensor (MCH/aptamer/PDA/Ag_2S/TiO_2NTs) was applied to PEC detection after incubation with different amounts of OFL for 60 min to form the aptamer-OFL complex (Scheme 1).

Photoelectrochemical methods

A three-electrode electrochemical cell, with a reference electrode of saturated calomel electrode, an auxiliary electrode of Pt sheet and a working electrode of modified TiO_2 NTs (0.25 cm^2), was applied to PEC measurements. Photocurrent was recorded in pH 7.0 PB comprising 0.1 M ascorbic acid using current-time curve method upon irradiation with visible-light at 10 s intervals. The working voltage was applied at 0 V.

Results and discussion

Characterization of the nanocomposites

The SEM morphologies of pure TiO_2NTs, Ag_2S/TiO_2NTs and PDA/Ag_2S/TiO_2NTs are shown in Fig. 1a–c. The pristine TiO_2 NTs displayed regularly round-shaped open structure (Fig. 1a). The inner diameter and wall thickness were about 80–100 nm *and* 10 *nm*, respectively. As shown in Fig. 1b, after depositing in situ by SILAR method, a great deal of spherical Ag_2S nanoparticles dispersed homogeneously on the nozzle of the nanotubes. The average particle size was about 10 nm. The PDA coated Ag_2S/TiO_2NTs exhibited inner diameter of 60–80 nm and wall thickness of about 20 nm (Fig. 1c), indicating that thin films of PDA were *formed on* both the outside and the inside tube walls of nanotubes via self-polymerization. The PDA coating layer uniformly decorated on the Ag_2S/TiO_2NTs, which endows the electrode with large specific surface area and a large number of active sites for immobilization of aptamers.

The structure of materials was studied using X-ray diffraction (XRD) technique. As depicted in Fig. 1d curve a, the diffraction peaks of anatase TiO_2 can be observed at 25.3°, 38.6°, 48°, 53.6° and 62.7°, which were related to the (101), (112), (200), (105) and (204) planes (JCPDS 71–1166) [11]. By comparison, the XRD pattern of Ag_2S/TiO_2NTs contained all diffraction peaks of TiO_2 NTs and displayed extra peaks at 28.97°, 34.39°, 40.74° in curve b, corresponding to the (111), (−121), (031) reflection of monoclinic phase of Ag_2S (JCPDS:14–0072) [13], indicating that Ag_2S nanoparticles were successfully modified on the surface of TiO_2NTs. After coating with PDA, no new diffraction peak appeared in curve c because PDA was amorphous polymer.

Figure 1e showed FT-IR spectra of TiO_2NTs, Ag_2S/TiO_2NTs and PDA/Ag_2S/TiO_2NTs. In curve a, pure TiO_2 NTs displayed its characteristic absorption peak at 600–1000 cm^{-1} due to the stretching vibrations of the Ti–O–Ti bond [11]. For Ag_2S/TiO_2NTs, no new absorption peaks in the entire infrared region appeared in curve b due to good infrared optical transmission properties of Ag_2S semiconductor nanoparticles. Compared to curve b, the FT-IR spectrum of PDA/Ag_2S/TiO_2NTs (curve c) exhibited new characteristic absorption peaks of the main functional groups in PDA. The corresponding peaks at 3051 cm^{-1}, 2956 cm^{-1}, 1611 cm^{-1} and 1230 cm^{-1} were ascribed to stretching vibration of -C-NH, C-H, C=C and C-N bond, respectively. The peak at 1503 cm^{-1} was attributed to the N-H bending vibration of PDA [33]. The above results further proved that PDA film was successfully modified on Ag_2S/TiO_2NTs.

Figure 1f presents diffuse reflectance UV-visible absorption spectrum (DRS) of the obtained nanocomposites. In the ultraviolet region, TiO_2 NTs exhibited a strong light absorption due to its wide band gap (curve a) [11]. After modification of Ag_2S nanoparticles, the DRS of Ag_2S/TiO_2NTs in curve b displayed an extended absorption edge of around 600 nm and stronger visible-light absorption. This phenomenon is ascribed to the high absorption coefficient and narrow band gaps of Ag_2S [12]. After sensitized with PDA, the color of the electrode surface was notably changed from pale purple to dark blue. Compared to Ag_2S/TiO_2NTs, PDA/Ag_2S/TiO_2NTs presented broadened and improved absorption in visible light region (curve c), implying that the PDA film can efficiently absorb the visible light due to the presence of conjugated polymer chains in PDA film [18]. The above results *confirm*ed that the co-sensitization effect of PDA/Ag_2S on TiO_2NTs can increase the visible-light harvesting, leading to enhancement of visible-light PEC activity of the PDA/Ag_2S/TiO_2NTs hybrid.

Characterization of the sensor

To study the PEC performance of PDA/Ag_2S/TiO_2NTs nanocomposites and monitor the fabrication process of aptasensor, the photocurrents on the electrodes formed in different fabrication steps were recorded in phosphate buffer comprising ascorbic acid (AA). In Fig. 2a curve a, a weak photocurrent of 3.0 μA was observed on the pure TiO_2 NTs electrode. For comparison, Ag_2S/TiO_2NTs composites displayed about 6-fold increase in photocurrent than TiO_2 NTs (curve b, I = 18.6 μA), demonstrating that the decoration of Ag_2S nanoparticles to the TiO_2 NTs can improve visible light harvesting capability and efficiently impede the charge carrier recombination of TiO_2 NTs which led to enhanced photoelectrochemical activity. After the PDA film was subsequently coated on Ag_2S/TiO_2NTs composite, the photocurrent signal reached about 10 times higher than that of pure TiO_2 NTs (curve c, I = 30.2 μA). The result demonstrated that PDA played an important role in enhancing absorption of constructed PEC sensor under visible

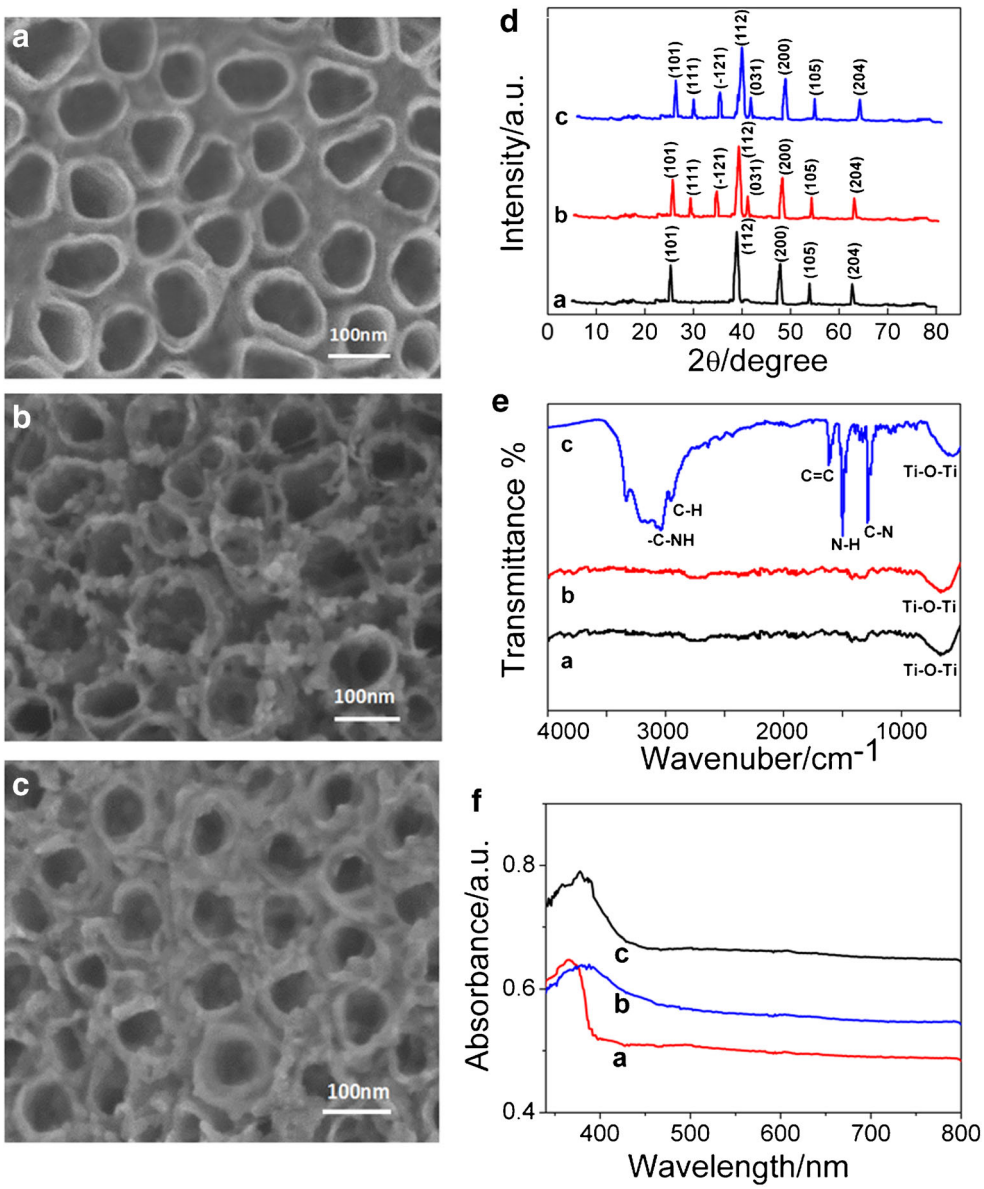

Fig. 1 SEM images of (**a**) TiO_2 NTs, **b** Ag_2S/TiO_2NTs and **c** PDA/Ag_2S/TiO_2NTs nanocomposite. **d** XRD patterns, **e** FT-IR spectra and **f** UV-visible diffuse reflectance spectra of (*a*) TiO_2 NTs, (*b*) Ag_2S/TiO_2NTs and (*c*) PDA/Ag_2S/TiO_2NTs

light and promoting the electron-hole separation, which can act as excellent organic sensitizer for the inorganic semiconductors to construct inorganic/organic photoactive composite material for PEC detection. Subsequently, the photocurrent notably decreased to 15.6 μA with the covalent immobilization of SH-terminated aptamer onto PDA/Ag_2S/TiO_2 NTs modified electrode via the Michael addition reaction (curve d), resulting from the steric hindrance effect of the immobilized aptamer and the electrostatic repulsion effect between the negative charged phosphate skeleton of aptamer and electronegative AA molecule. After successive blocking of MCH (curve e) and specific binding of OFL, photocurrent gradually decreased because the increased stereo-hindrance can prevent AA from combining with photo-generated holes and facilitate the recombination of photogenerated holes/electrons. As a result, when the 100 nM of OFL was connected with aptamer by the specific recognition, the photocurrent value obviously reduced to 7.0 μA (curve f). These phenomena indicated that the PEC aptasensor based on PDA/Ag_2S/TiO_2NTs nanocomposites was successfully constructed for the detection of OFL.

Electrochemical impedance spectroscopy (EIS) was applied to characterize the interface properties of electrodes. Figure 2b displayed impedance spectra for the electrodes acquired from different fabrication process. The Nyquist plot of EIS is composed of a semicircle section and a line section. The electron-transfer resistance (R_{et}) can be reflected by the semicircle diameter [5]. In comparison to TiO_2 NTs electrode (curve a), Ag_2S/TiO_2NTs showed increased resistance ascribed to the poor conductivity of Ag_2S semiconductor nanoparticles (curve b). In curve c, the PDA/Ag_2S/TiO_2NTs modified electrode showed much higher R_{et} owing to the relatively low conductivity of PDA which retarded the interfacial

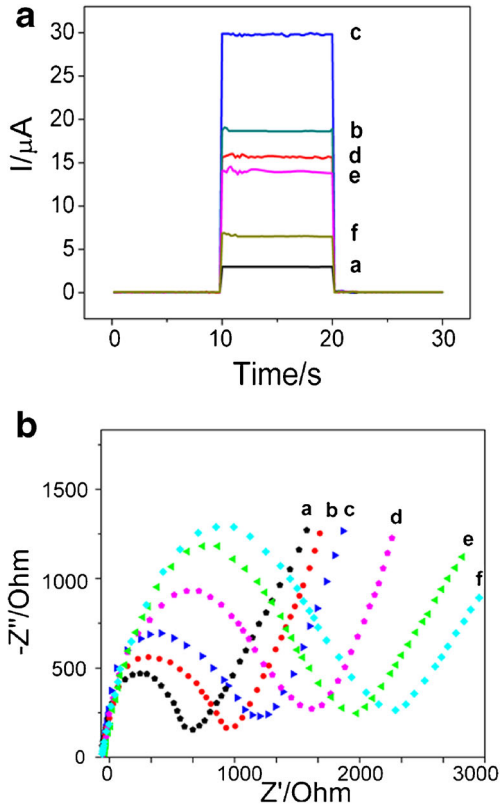

Fig. 2 PEC response (**a**) and EIS (**b**) for (*a*) TiO_2 NTs, (*b*) Ag_2S/TiO_2NTs, (*c*) PDA/Ag_2S/TiO_2NTs, (*d*) aptamer/ PDA/Ag_2S/TiO_2NTs, (*e*) MCH/aptamer/ PDA/Ag_2S/TiO_2NTs, (*f*) OFL/MCH/aptamer/ PDA/Ag_2S/TiO_2NTs. **c** The charge transport mechanism of PDA/Ag_2S/TiO_2NTs electrode in AA electrolyte upon irradiation with visible light

electron transfer [17]. After immobilizing aptamer onto the surface of PDA/Ag_2S/TiO_2NTs, the semicircle diameter evidently enhanced (curve d), implying that aptamers were successfully attached to the PDA/Ag_2S/TiO_2 NTs by the Michael addition reaction between PDA and SH groups of the aptamer [8]. Subsequent modification of MCH led to further augmentation of the electron transfer resistance due to surface blocking effect (curve e). After the incubation of aptasensor with OFL, there was a remarkable increase of the semicircle diameter (curve f) because aptamer-OFL complexes blocked interfacial charge transfer. The EIS characterization also pointed to the successful construction of aptasensor.

Figure 2c presents the charge transport pathway of PDA/Ag_2S/TiO_2NTs hererostructure upon irradiation with visible light. In the process of photo-current conversion, after the PDA thin film absorbs visible light, electron-hole pairs are generated in the PDA under the photoexcitation [16]. Then the excited electrons on the lowest unoccupied molecular orbital (LUMO) of PDA can transfer onto the conduction band (CB) of Ag_2S nanoparticles due to well-matched energy level. Because the valence band (VB) and CB energy levels of Ag_2S nanoparticles are higher than those of TiO_2 NTs, the photogenerated electrons subsequently inject into the CB of TiO_2 NTs to generate current in external circuit. The separated holes transfer from the VB of TiO_2 NTs to the highest occupied molecular orbital (HUMO) of PDA through the VB of Ag_2S nanoparticles, resulting in oxidization of AA in PB. Because the photogenerated holes are consumed by the electron donor AA, the recombination of photogenerated electron–hole pairs can be effectively inhibited. Therefore, the photocurrent response of electrode evidently enhanced. The photocurrent change tendency of different modified electrode in Fig. 2a curve a-c is well in accordance with the above charge transfer mechanism which further confirmed that

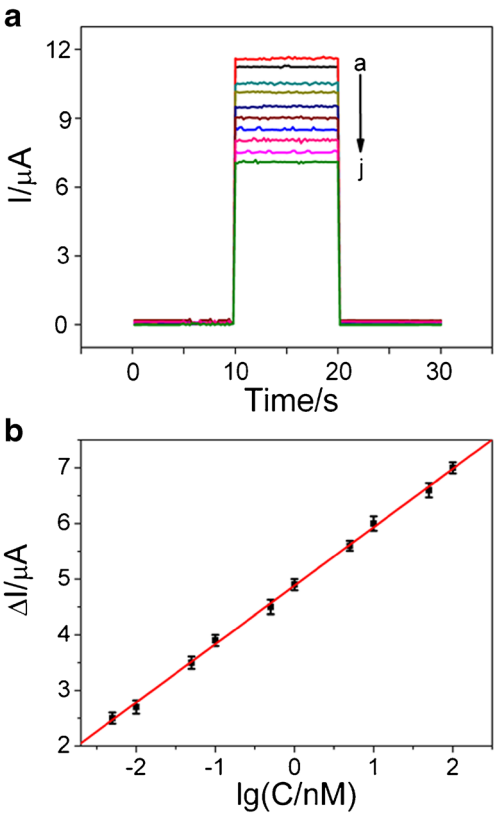

Fig. 3 **a** Photocurrent response towards various concentrations of OFL. (*a*) 0.005, (*b*) 0.01, (*c*) 0.05, (*d*) 0.1 (*e*) 0.5, (*f*) 1.0, (*g*) 5.0, (*h*)10, (*i*) 50, (*j*) 100 nM. **b** Logarithmic calibration plot between photocurrent change (ΔI) and concentration of OFL

Table 1 Comparison of various methods for OFL assay

Methods	Linear range (M)	Detection limit (M)	Reference
DCBI-MS	3.4×10^{-6}-1.7×10^{-4}	3.2×10^{-7}	[23]
UHPLC–MS/MS	2.7×10^{-10}-2.7×10^{-8}	2.7×10^{-10}	[24]
Chemiluminescence sensor	2.8×10^{-9}-2.8×10^{-6}	8.4×10^{-10}	[25]
Electrochemical sensor	1.0×10^{-6}-1.0×10^{-4}	1.3×10^{-6}	[26]
Electrochemical immunosensor	2.2×10^{-10}-1.1×10^{-6}	8.3×10^{-11}	[27]
Electrochemical aptasensor	5.0×10^{-8}-2.0×10^{-5}	1.0×10^{-9}	[28]
Colorimetric aptasensor	2.0×10^{-8}- 4.0×10^{-7}	3.4×10^{-9}	[29]
Fluorescence detection	2.8×10^{-9}-1.4×10^{-6}	5.8×10^{-10}	[30]
Photoelectrochemical aptasensor	5.0×10^{-12}-1.0×10^{-7}	7.5×10^{-13}	This work

DCBI-MS: Desorption corona beam ionization - mass spectrometry; UHPLC–MS/MS: Ultra-high performance liquid chromatography-tandem mass spectrometry

$PDA/Ag_2S/TiO_2NTs$ hererostructure exhibited distinctly enhanced visible-light PEC activity contributing to well-matched energy levels, ideal stepwise band structure and excellent co-sensitization effect of PDA/Ag_2S on TiO_2NTs.

Optimization of experimental conditions

The following experimental conditions including the modification amount of Ag_2S nanoparticles and PDA on TiO_2NTs, the concentration of AA, immobilization amount of aptamer, incubation time of OFL were systemically optimized (presented in Electronic Supporting Material). The optimized conditions were found as follows: (a) Modification amount of Ag_2S nanoparticles: depositing time of 60 s and loading cycles of 4 cycles (b) Modification amount of PDA: DA concentration of 3.0 $mg \cdot mL^{-1}$ and polymerization time of 2 h; (c) Concentration of AA: 0.1 M; (d) Immobilization amount of aptamer: 2.0 μM; (e) Incubation time: 1 h.

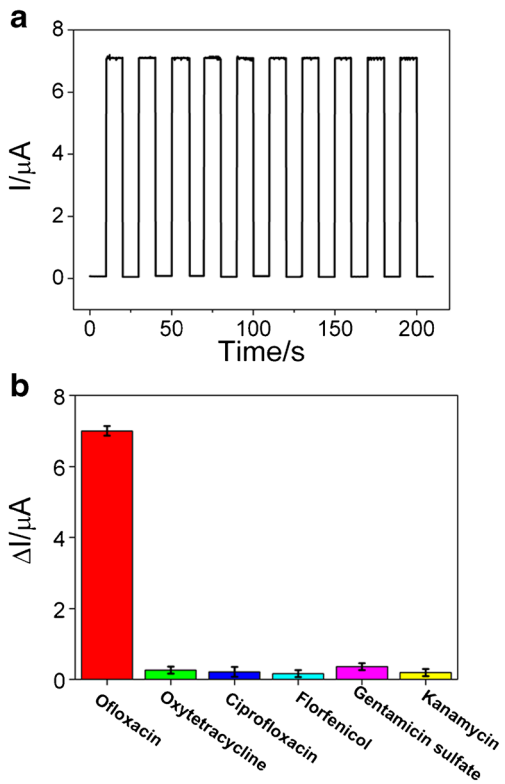

Fig. 4 **a** Time-based photocurrent response of the aptasensor under ten on/off irradiation cycles. **b** Selectivity detection for OFL (10 nM) and other interferential antibiotics (100 nM)

Quantitative determination of OFL

After incubation of the aptasensor in different concentrations of OFL, photocurrent responses were recorded under the optimal conditions. As shown in Fig. 3a, the decreased photocurrent responses were observed in presence of increased OFL levels. The difference of photocurrent after and before incubation with OFL (ΔI) was used as detection signal for quantitative analysis. Under the optimized conditions, the aptasensor has a linear response in the 5.0 pM to 100 nM OFL concentration range (Fig. 3b) and a 0.75 pM detection limit (at $S/N = 3$). The regression equation is expressed as ΔI (μA) =4.883 + 0.1049 lg (c/nM), and the linear correlation coefficient is 0.9991.The comparison of analytical properties of various methods for OFL assay are summarized in Table 1. Although the fabrication process of aptasensor is intricate and time-consuming, this method possesses high sensitivity and wide linear range, indicating its excellent analytical performance towards OFL detection.

Table 2 Detection of OFL in milk samples ($n = 6$)

Sample	Added (pM)	Found (pM)	Recovery (%)	RSD (%)
1	50	49.1	98.2	3.5
2	100	97.6	97.6	3.3
3	500	494.9	99.0	3.0

Reproducibility, stability and specificity

To evaluate the reproducibility, five parallel fabricated aptasensors were used to determine 100 nM of OFL. The photocurrent response offered relative standard deviation (RSD) of 2.8%, indicating favorable reproducibility for OFL assay. As can be seen in Fig. 4a, the photocurrent did not significantly change (with a RSD of 2.5%) when recorded at 10 intervals of visible light, implying desirable stability of the PEC response.

To investigate the binding specificity of the aptasensor for its target analyte, interference experiments were performed by using the nanoprobe to individually detect target OFL and other non-target antibiotics at same experimental conditions. The results demonstrate that OFL revealed large photocurrent response, whereas 10-fold of interfering substances brought out no significant photocurrent change (Fig. 4b), indicating the good selectivity of aptasensor for OFL detection.

Analysis of food samples

The feasibility of this method for food analysis was assessed. The spiked milk samples containing different amounts of OFL were prepared according to the protocol reported previously [5]. Then, the standard addition method was used to detect OFL in milk sample. The obtained concentration recovery was between 97.6% and 99.0% (Table 2), indicating the applicability of this aptasensor in complex food samples.

Conclusions

A PDA/Ag_2S/TiO_2NT ternary nanocomposite was firstly synthesized and used to construct novel PEC aptasensing platform. The inorganic/organic photoactive materials not only exhibit distinctly enhanced visible-light PEC activity but also offer an ideal platform to directly bind the aptamer to fabricate aptasensor for OFL detection. Although the fabrication process of aptasensor is intricate and time-consuming, this method possesses high sensitivity and good selectivity, which holds great potentials for OFL residue analysis in real samples.

Compliance with ethical standards The author(s) declare that they have no competing interests.

References

1. Zhao WW, Xu JJ, Chen HY (2016) Photoelectrochemical aptasensing. Trends Anal Chem 82:307–315
2. Wang GL, Shu JX, Dong YM, Wu XM, Zhao WW, Xu JJ, Chen HY (2015) Using G-quadruplex/hemin to "switch-on" the cathodic photocurrent of p-type PbS quantum dots: toward a versatile platform for photoelectrochemical aptasensing. Anal Chem 87: 2892–2900
3. Liu S, Xing XR, Yu JH, Lian WJ, Li J, Cui M, Huang JD (2012) A novel label-free electrochemical aptasensor based on graphene–polyaniline composite film for dopamine determination. Biosens Bioelectron 36:186–191
4. Du Y, Dong SJ (2017) Nucleic acid biosensors: recent advances and perspectives. Anal Chem 89:189–215
5. Wang Y, Bian F, Qin XF, Wang QQ (2018) Visible light photoelectrochemical aptasensor for sensitive detection of chloramphenicol based on trivalent Eu-doped CdS quantum dots-sensitized TiO_2 nanorod array. Microchim Acta 185:161
6. Wang GL, Gu TT, Dong YM, Wu XM, Li ZJ (2015) Photoelectrochemical aptasensing of lead(II) ion based on the in situ generation of photosensitizer of a self-operating photocathode. Electrochem Commun 61:117–120
7. Qin XF, Wang QQ, Geng LP, Shu XL, Wang Y (2019) A "signal-on" photoelectrochemical aptasensor based on graphene quantum dots -sensitized TiO_2 nanotube arrays for sensitive detection of chloramphenicol. Talanta 197:28–35
8. Li HN, Zhu MY, Chen W, Wang K (2017) Ternary heterojunctions composed of BiOCl, $BiVO_4$ and nitrogen-doped carbon quantum dots for use in photoelectrochemical sensing: effective charge separation and application to ultrasensitive sensing of dopamine. Microchim Acta 184:4827–4833
9. Shankar K, Basham JI, Allam NK, Varghese OK, Mor GK, Feng X (2009) Recent advances in the use of TiO_2 nanotube and nanowire arrays for oxidative photoelectrochemistry. J Phys Chem C 113: 6327–6359
10. Lee YL, Chi CF, Liau SY (2010) CdS/CdSe co-sensitized TiO_2 Photoelectrode for efficient hydrogen generation in a Photoelectrochemical cell. Chem Mater 22:922–927
11. Chen YL, Tao Q, Fu WY, Yang HB, Zhou XM, Su S, Ding D, Mu YN, Li X, Li MH (2014) Enhanced photoelectric performance of PbS/CdS quantum dot co-sensitized solar cells via hydrogenated TiO_2 nanorod arrays. Chem Commun 50:9509–9512
12. Kalpana K, Selvaraj V (2016) Thiourea assisted hydrothermal synthesis of ZnS/CdS/Ag_2S nanocatalysts for photocatalytic degradation of Congo red under direct sunlight illumination. RSC Adv 6: 4227–4236
13. Gholami M, Qorbani M, Moradlou O, Naseri N, Moshfegh AZ (2014) Optimal Ag_2S nanoparticle incorporated TiO_2 nanotube array for visible water splitting. RSC Adv 4:7838–7844
14. Neves MC, Nogueira JMF, Trindade T, Mendonça MH, Pereira MI, Monteiro OC (2009) Photosensitization of TiO_2 by Ag_2S and its catalytic activity on phenol photodegradation. J Photochem Photobiol A Chem 204:168–173
15. Lee H, Dellatore SM, Miller WM, Messersmith PB (2007) Mussel-inspired surface chemistry for multifunctional coatings. Science 318:426–430
16. Nam HJ, Kim B, Ko MJ, Jin M, Kim JM, Jung DY (2012) A new mussel-inspired polydopamine sensitizer for dye-sensitized solar cells: controlled synthesis and charge transfer. Chem Eur J 18: 14000–14007
17. Wang GX, Xu QJ, Liu L, Su XL, Lin JH, Xu GY, Luo XL (2017) Mixed self-assembly of polyethylene glycol and aptamer on polydopamine surface for highly sensitive and low-fouling detection of adenosine triphosphate in complex media. ACS Appl Mater Interfaces 9:31153–31160
18. Yang Y, Hu WH (2017) Bifunctional polydopamine thin film coated zinc oxide nanorods for label free photoelectrochemical immunoassay. Talanta 166:141–147
19. Stolker AAM, Brinkman UAT (2005) Analytical strategies for residue analysis of veterinary drugs and growth-promoting agents in food-producing animals: a review. J Chromatogr A 1067:15–53

20. Monk J, Campoli-Richards D (1987) Ofloxacin: a review of its antibacterial activity, pharmacokinetic properties and therapeutic use. Drugs 33:346–391
21. Sun WY, Liu WY, Qu LB (2007) Development of ELISA and immunochromatographic assay for Ofloxacin. Chin Chem Lett 18:1107–1110
22. Sun HW, He P, Lv YK, Liang SX (2007) Effective separation and simultaneous determination of seven fluoroquinolones by capillary electrophoresis with diode-array detector. J Chromatogr B 852: 145–151
23. Wang H, Li LH, Xing R, Zhang YY, Wu TT, Chen B, Li ZX, Fei ZH, Liu ZM, Ding H (2019) Screening of antimicrobials in animal-derived foods with desorption corona beam ionization (DCBI) mass spectrometry. Food Chem 272:411–417
24. Li J, Ren XL, Diao YY, Chen Y, Wang QL, Jin WT, Zhou P, Fan QQ, Zhang YB, Liu HM (2018) Multiclass analysis of 25 veterinary drugs in milk by ultra-high performance liquid chromatography-tandem mass spectrometry. Food Chem 257: 259–264
25. Liu W, Guo YM, Li HF, Zhao M, Lai ZS, Li BX (2015) A paper-based chemiluminescence device for the determination of ofloxacin. Spectrochim Acta A 137:1298–1303
26. Si XJ, Wei YL, Wang CL, Li L, Ding YP (2018) A sensitive electrochemical sensor for ofloxacin based on a graphene/zinc oxide composite film. Anal Methods 10:1961–1967
27. Zang S, Liu YJ, Lin MH, Kang JL, Sun YM, Lei HT (2013) A dual amplified electrochemical immunosensor for ofloxacin: Polypyrrole film-Au nanocluster as the matrix and multi-enzyme-antibody functionalized gold nanorod as the label. Electrochim Acta 90:246–253
28. Pilehvar S, Reinemann C, Bottari F, Vanderleyden E, Vlierberghe SV, Strehlitz B, Wael KD (2017) A joint action of aptamers and gold nanoparticles chemically trapped on a glassy carbon support for the electrochemical sensing of ofloxacin. Sensors Actuators B Chem 240:1024–1035
29. Zhou XT, Wang LM, Shen GQ, Zhang DW, Xie JL, Mamut A, Huang WW, Zhou SS (2018) Colorimetric determination of ofloxacin using unmodified aptamers and the aggregation of gold nanoparticles. Microchim Acta 185:355
30. Mirzajani R, Pourreza N, Burromandpiroze J (2018) Fabrication of magnetic Fe_3O_4@nSiO_2@mSiO_2–NH_2 core–shell mesoporous nanocomposite and its application for highly efficient ultrasound assisted dispersive μSPE-spectrofluorimetric detection of ofloxacin in urine and plasma samples. Ultrason Sonochem 40:101–112
31. Qiao JL, Wang QY, Ye JX, Xiao YK (2016) Enhancing photoelectrochemical performance of TiO_2 nanotube arrays by CdS and Bi_2S_3 co-sensitization. J Photochem Photobiol A 319(320):34–39
32. Wang QY, Jin RC, Yin CL, Wang MJ, Wang JF, Gao SM (2017) Photoelectrocatalytic removal of dye and Cr(VI) pollutants with Ag_2S and Bi_2S_3 co-sensitized TiO_2 nanotube arrays under solar irradiation. Sep Purif Technol 172:303–309
33. Dai J, Shi C, Li C, Shen X, Peng L, Wu D, Sun D, Zhang P, Zhao J (2016) A rational design of separator with substantially enhanced thermal features for lithium-ion batteries by the polydopamine-ceramic composite modification of polyolefin membranes. Energy Environ Sci 9:3252–3261